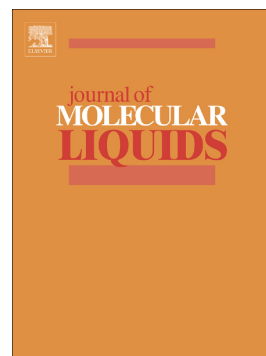


## Accepted Manuscript

Novel high throughput mixed matrix membranes embracing poly ionic liquid-grafted biopolymer: Fabrication, characterization, permeation and antifouling performance

Reda F.M. Elshaarawy, Janina Dechnik, Hassan M.A. Hassan, Dennis Dietrich, Mohamed A. Betiha, Stephan Schmidt, Christoph Janiak



PII: S0167-7322(18)32781-8  
DOI: [doi:10.1016/j.molliq.2018.06.100](https://doi.org/10.1016/j.molliq.2018.06.100)  
Reference: MOLLIQ 9298  
To appear in: *Journal of Molecular Liquids*  
Received date: 28 May 2018  
Revised date: 22 June 2018  
Accepted date: 25 June 2018

Please cite this article as: Reda F.M. Elshaarawy, Janina Dechnik, Hassan M.A. Hassan, Dennis Dietrich, Mohamed A. Betiha, Stephan Schmidt, Christoph Janiak , Novel high throughput mixed matrix membranes embracing poly ionic liquid-grafted biopolymer: Fabrication, characterization, permeation and antifouling performance. Molliq (2018), doi:[10.1016/j.molliq.2018.06.100](https://doi.org/10.1016/j.molliq.2018.06.100)

This is a PDF file of an unedited manuscript that has been accepted for publication. As a service to our customers we are providing this early version of the manuscript. The manuscript will undergo copyediting, typesetting, and review of the resulting proof before it is published in its final form. Please note that during the production process errors may be discovered which could affect the content, and all legal disclaimers that apply to the journal pertain.

## Novel high throughput mixed matrix membranes embracing poly ionic liquid-grafted biopolymer: fabrication, characterization, permeation and antifouling performance

Reda F.M. Elshaarawy<sup>a,b,\*</sup>, Janina Dechnik<sup>a</sup>, Hassan M. A. Hassan<sup>b</sup>, Dennis Dietrich<sup>a</sup>, Mohamed A. Betiha<sup>c</sup>, Stephan Schmidt<sup>d</sup>, Christoph Janiak<sup>a,\*</sup>

<sup>a</sup> Anorganische Chemie und Strukturchemie Institut, Heinrich-Heine Universität Düsseldorf, 40204 Düsseldorf, Germany.

<sup>b</sup> Faculty of Science, Suez University, Suez, Egypt.

<sup>c</sup> Egyptian Petroleum Research Institute, Nasr City, Cairo 11727, Egypt

<sup>d</sup> Department of Colloidal Adhesion, Organic and Macromolecular Chemistry Institute, Heinrich-Heine Universität Düsseldorf, 40225 Düsseldorf, Germany.

\* Corresponding authors

Email: [reda.elshaarawy@suezuniv.edu.eg](mailto:reda.elshaarawy@suezuniv.edu.eg); [reel-001@hhu.de](mailto:reel-001@hhu.de)

Email: [janiak@hhu.de](mailto:janiak@hhu.de)

### Abstract

We report a simple and effective protocol for preparation of a poly-ionic liquid (PIL)-grafted chitosan Schiff base (**PILCSB**) and titanium oxide nanoparticles (TNPs) for application as an antibiofouling nanocomposite in the fabrication of new polysulfone (PSU) ultrafiltration mixed matrix membranes (MMMs). The effect new additive (**PILCSB@TNPs**) on the porosity texture, pure water flux (PWF) and antibiofouling profile for modified MMMs was investigated. Interestingly, the surface hydrophilicity of these MMMs was remarkably enhanced in comparison to the neat PSU membrane (M0) as revealed from wettability and water contact- angle results (wettability/ water contact angle = 29.18%/ 93.48° and 83.46%/ 57.35° for M0 and MMM6, respectively).

**Keywords:** Mixed matrix membranes; PIL-grafted biopolymer; Nanocomposite; Antibiofouling; Water flux.

### 1. Introduction

During last few decades, the worldwide population has quadrupled while global water demands grown seven-fold [1]. Where by the end of 2030, 3.9 billion people will suffer

strongly from water scarcity as predicted by the World Water Council [2]. Therefore, water scarcity along with poor water quality is a dormant crisis about to explode worldwide. One of the most promising efforts to stem the global water crisis is the domestic and industrial wastewater reclamation. Membrane technologies are favored over many other technologies for purification of water due to their unmatched features such as mild operating conditions, no chemical additives or thermal inputs requirements, efficient, selective, reliable separations and eco-friendliness [3].

Outstanding physicochemical features of polysulfone (PSU) including excellent thermal, chemical, oxidative and hydrolytic stability with preserving its constancy toward pH-fluctuation [4,5], superior mechanical properties such as toughness, strength, rigidity and flexibility along with good film forming characteristic [4,6] put it in the forefront of attention of many researchers for manufacturing of diverse membranes [4,7]. However, the wide-ranging applications of PSU in water treatment are often limited by its inherent hydrophobicity and non-wetting characteristics that facilitate the hydrophobic interaction, deposition and adsorption between the surface of PSU membranes and microorganisms or lipophilic foulants in the feed solution which in turn leads to serious membrane biofouling [8,9] resulting in poor permeation and diminishing of permeate flux, increasing maintenance costs, alteration of membrane selectivity and durability. Therefore, there is growing demand for fabrication of antifouling UF membranes through an enhancement of the hydrophilicity of PSU surface *via* physical or chemical refinements. So far, surface grafting, surface coating and blending are the most common techniques employed for enhancing membrane surface hydrophilicity and antifouling efficacy, accordingly [10,11]. Recently, surface modification by blending of the host membrane matrix with hydrophilic or amphiphilic macromolecular additives revealed it as a simple and an effective method for fabrication of hydrophilic antibiofouling membranes [12]. For instance, Poly-(ethylene glycol)-based and polyzwitterionic architectures of significant hydration capacity are effectively used as hydrophilicity fine-tuning additives [13].

Among natural biopolymers, chitosan (CS), a copolymer of glucosamine (GlcNH<sub>2</sub>) and N-acetylglucosamine (GlcNHAc) blocks, can offer a key starting material for fabrication of ideal promising eco-friendly membrane antibiofouling modulators owing to its wide-spectrum antialgal, antimicrobial efficacies [14], amazing antibiofouling properties [15], and superior film-forming ability. Furthermore, CS offers a green protocol to combat biofouling as it is produced by mining of marine wastes (e.g., shrimp- and crab-shells) [16]. However, application of neat CS for the blended membrane technology is restricted due to its limited

solubility and lower thermo-mechanical stability [17]. Thus, surface-functionalization of CS was addressed to overcome these aforementioned challenges and construct surface-functionalized CS which may act as a key contributor for improving the hydrophilicity and antibiofouling behaviors of UF membranes [18,19].

Notable, polymeric ionic liquids (PILs) have been used to fabricate diverse “smart” materials [20,21] for various applications in gas separation, membranes technologies, electrochemical energy devices, antimicrobials, catalysis, stimuli-responsive materials, carbon materials, sensors [22] and wettability-switchable materials [23]. Recent works revealed that surface functionalization of membrane with PIL brushes can offer undeniable engineering and economic advantages over the native membrane including tunable charge, wettability and antifouling properties. For instance, Ye *et al* [24] and others [25,26] reported that PIL brushes could be reversibly switched the surface wettability from hydrophilicity to hydrophobicity and synergistically enhanced the antimicrobial and antifouling properties of the surface as compared with traditionally polymer terminals. Moreover, the antimicrobial and antibiofouling efficacies of PIL brushes could be fine-tuned by exchanging their counter anions. Interestingly, the hexafluorophosphate-based poly(ionic liquid) coated Titania nanoparticles (TNPs) exhibited excellent antibacterial activity in comparison with pristine TiO<sub>2</sub> NPs. Moreover, TNPs-based membranes displayed superior antibacterial, photocatalytic effects [27] and enhanced antifouling performance [28].

Inspired by previous outstanding facts and in our endeavor toward the designing and fabrication of novel architectures for bioapplications [14a,15a,29] we aimed in this work to design a simple efficient protocol for preparing an eco-friendly anti-biofoulant (based on a poly-ionic liquids-grafted chitosan Schiff base, PILCSB) and TNPs as synergistic (anti-microbial and anti-biofouling) modulator for a PSU membrane (Fig. 1) which may significantly improve the anti-biofouling and filtration performance of new MMMs.

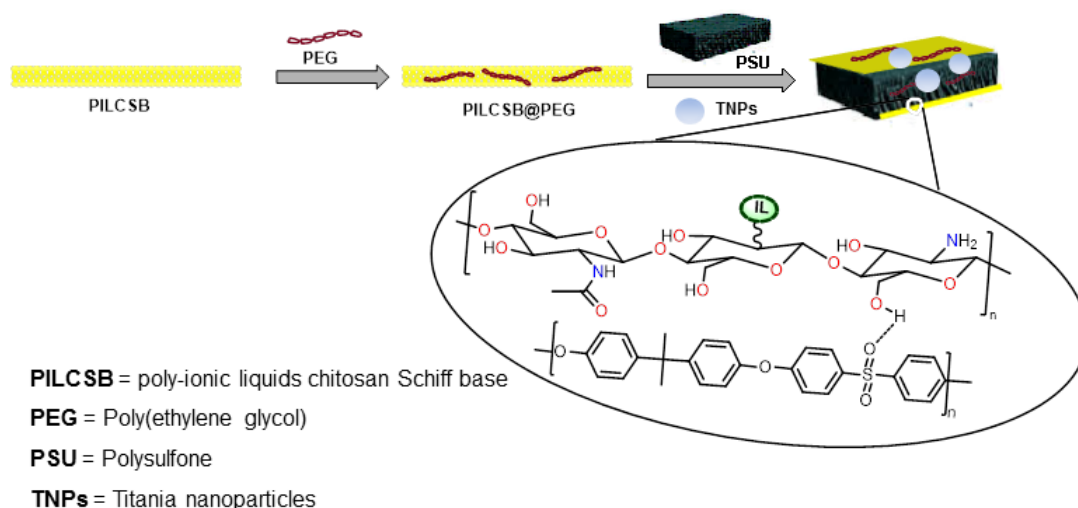


**Fig. 1:** Diagrammatic representation for the functionalization of the PSU surface with PILCSB, PEG and TNPs to fabricate the target MMMs, PSU@PILCSB@PEG@TNPs.

## 2. Materials and methods

Instrumentation, sources of materials, extraction of CS from shrimp shells and preparation details of TNPs and 4-methoxypyridinium ethoxysalicylaldehyde ionic liquid ((EtO)Sal-MeOPy<sup>+</sup>X<sup>-</sup>, **3a,b**) are available in the electronic supplementary information (ESI†).

### 2.1. Synthesis of 5-(4-methoxypyridinium hexafluorophosphate)-ethoxysalicylidene chitosan (PILCSB)

CS (1 g) was dissolved in 100 mL of a mixture of ethanol and 1% aqueous acetic acid (1:1 v/v) by stirring at 50 °C for 30 min. (EtO)Sal-MeOPy<sup>+</sup>PF<sub>6</sub><sup>-</sup>, **3b** (equivalent to the NH<sub>2</sub>-content in CS) was dissolved in a hot ethanol (30 mL) and then the obtained solution was added portionwise to a stirring homogeneous solution of CS over a time of 30 min at the same temperature. Then, the reaction temperature was raised to 80 °C and the reaction mixture was further stirred at this temperature for 24 h. The desired product was isolated from the reaction media by adding an excessive amount of ethyl acetate (AcOEt) coupled with ultrasonication at r.t. for 5 h. The obtained product (**PILCSB**) was filtered and then washed with EtOH:AcOEt mixtures (30:70, 20:80, and 0:100 v/v) (3 x 10 mL). Finally, **PILCSB** was dried under vacuum at 40 °C for 24 h to obtain the desired PILCSB: It is obtained as a yellowish-orange powder, Yield (2.13 g, 97.9%). FTIR (KBr, cm<sup>-1</sup>): 3445 (vs, br), 3211 (m, br), 1658 (s, sh), 1636 (vs, sh), 1532 (m, sh), 1379 (m, sh), 1284 (m, sh), 1158 (s, sh), 1065 (m, sh), 896 (m, sh), 836 (s, sh) 767, 656 (m, sh). <sup>1</sup>H NMR (600 MHz, 1% CD<sub>3</sub>COOD/D<sub>2</sub>O)<sub>60 °C</sub> δ (ppm): 11.23 (s, 1H), 10.89 (s, 1H), 8.92 (d, *J* = 7.1 Hz, 2H), 8.51 (d,

$J = 7.3$  Hz, 4H), 8.28 (d,  $J = 7.2$  Hz, 1H), 7.99 (d,  $J = 8.3$  Hz, 4H), 7.80-7.67 (m, 4H), 5.95 (s, 4H), 5.23 (d,  $J = 7.6$  Hz, 1H), 4.39 (q, 4H), 4.14 (br, s, 2H), 4.01 (s, 6H), 3.91-3.79 (m, 2H), 3.65 (t,  $J = 7.1$  Hz, 2H), 3.53 (br, s, 2H), 3.32-3.19 (m, 4H), 2.78 (t,  $J = 8.1$  Hz, 2H), 2.45 (dd,  $J = 13.8, 8.4$  Hz, 3H), 1.39 (t,  $J = 7.6$  Hz, 6H).  $^{13}\text{C}$  NMR (151 MHz, 1%  $\text{CD}_3\text{COOD}/\text{D}_2\text{O}$ ) $_{60^\circ\text{C}}$   $\delta$  (ppm): 178.35, 178.10, 176.61, 164.55, 163.28, 153.48, 152.26, 151.18, 150.03, 148.49, 148.14, 147.26, 146.31, 134.85, 134.09, 127.86, 126.91, 118.99, 118.19, 110.77, 109.88, 109.11, 89.71, 85.42, 83.36, 81.51, 80.49, 79.13, 78.22, 76.26, 75.63, 75.21, 74.37, 73.45, 72.28, 71.31, 71.10, 68.34, 65.43, 65.18, 62.06, 58.38, 56.41, 19.89 and 18.63.  $^{31}\text{P}$  NMR (202 MHz,  $\text{DMSO}-d_6$ ): -159.38 to -117.33 ppm (septet,  $^2J_{\text{PF}} = 711.18$  Hz).  $^{19}\text{F}$  NMR (470 MHz,  $\text{DMSO}-d_6$ ): -67.81 to -64.78 ppm (doublet,  $^1J_{\text{PF}} = 711.24$  Hz).

## 2.2. Preparation of neat PSU membrane (M0)

All membranes have been fabricated *via* modified non-solvent induced phase inversion (NSIPI) and slow evaporation methods. To prepare the casting solution, a certain amount (3.8 g) of PSU was dissolved in NMP (15.2 g, 15.66 mL) under vigorous stirring at 60 °C to obtain a homogeneous PSU solution which was further stirred at 300 rpm for 8 h. Then, the casting solution was debubbled using vacuum for 15 min. Afterwards, the bubble-free solution was then casted on either a nonwoven polyester fabric (novatex2483) and immediately exposed to warmed water vapor for 15 min and then immersed into a milli-Q water as a non-solvent at r.t. for NSIPI, or onto 2.5 cm Petri dishes, for slow evaporation in vacuum oven at 50 °C/ 2 days. Noteworthy, the membranes obtained by NSIPI should be stored in a milli-Q water for 3 days for complete removal of a residual NMP.

## 2.3. Fabrication of UF MMMs (MMM1, MMM2, MMM4, MMM5)

General procedure to fabricate PSU@CS (MMM1) and PSU@PILCSB (MMM4) membranes (see Table 1 for the membrane composition) is described as follows: A 2% solution of CS is obtained by dissolving 1 g CS in 50 mL of 1% aqueous AcOH (solution of PILCSB obtained by dissolving 0.10 g in 5 mL NMP). PSU (3.8 g) was dissolved in (9.20 g, 9.50 mL) of NMP by stirring at 60 °C for 4h to obtain a clear homogeneous solution. Then, 5.0 mL of the obtained CS or **PILCSB** solution was added dropwise to the PSU solution under vigorous stirring at 1100 rpm, maintaining the temperature at 60 °C. Thereafter, further 0.93 mL (0.90 g) of NMP was added. While CS was being added, it is re-precipitated resulting in a formation of turbid solution which was stirred vigorously, at 900 rpm, at 70 °C

for 12 h to obtain clear viscous casting solution. Then, this casting solution was deaerated under vacuum to obtain bubbles-free casting solution. Afterwards, the bubble-free solution was then casted on either a nonwoven polyester fabric (novatex2483), for NSIPI, or onto 2.5 cm petri dishes, for slow evaporation, as described above. The fabricated MMMs were washed several times with distilled water and then milli-Q water before being dried at 30 °C. Similar procedures were employed for the preparation of the PSU@CS@PEG (MMM2) and PSU@PILCSB@PEG (MMM5) membranes by replacing definite amount of NMP with equivalent amount of PEG.

**Table 1.** Composition (W %) of the prepared MMMs.<sup>†</sup>

Membrane ID	PSU	NMP	AcOH	PEG	CS	PILCSB	TNPs
M0	20.0	80.0	–	–	–	–	–
MMM1	20.0	53.2	26.3	–	0.5	–	–
MMM2	20.0	53.0	26.3	0.2	0.5	–	–
MMM3	20.0	52.9	26.3	0.2	0.5	–	0.1
MMM4	20.0	79.5	–	–	–	0.5	–
MMM5	20.0	79.3	–	0.2	–	0.5	–
MMM6	20.0	79.2	–	0.2	–	0.5	0.1

<sup>†</sup> PSU, polysulfone; MMM, mixed matrix membrane; NMP, N-methyl-2-pyrrolidone; AcOH, 1% acetic acid; CS, chitosan; PEG, polyethylene glycol; TNPs, TiO<sub>2</sub> nanoparticles.

#### 2.4. Fabrication of nanocomposite mixed matrix membranes (MMM3) and (MMM6)

Generally, 2 wt% solutions of CS (2 g/100 mL) and PILCSB were prepared by dissolving 0.1 g of CS and PILCSB, separately, in 5 mL of 1 wt% aqueous acetic acid and 5 mL of NMP, respectively. To these solutions, PEG was added with continuous stirring at 500 rpm to obtain CS@PEG and PILCSB@PEG. Then, two equal amounts (3.8 g) of PSU were dissolved separately in two quantities (9.20 g, 9.50 mL) of NMP by stirring at 60 °C/ 500 rpm for 4 h to obtain two homogenous solutions. Afterwards, previously prepared CS@PEG and PILCSB@PEG solutions were added separately to the PSU solutions under vigorous stirring, 1100 rpm, at 60 °C. Then, additional 0.93 mL (0.90 g) of NMP was added. The obtained turbid solution was vigorously stirred at 70 °C for 12 h to obtain clear highly viscous solutions. Thereafter, TNPs were added to these solutions under continuous stirring at 60 °C for 1h followed by sonication for 1 h at the same temperature. Then, the casting solutions were deaerated under vacuum and casted on either a nonwoven polyester fabric (novatex2483), for NSIPI, or onto 2.5 cm petri dishes, for slow evaporation, as described above.

## 2.5. Membranes structural and surface characterization

### 2.5.1. ATR-IR analysis

Attenuated Total Reflection-Fourier Transform Infrared Spectroscopy (ATR-FTIR) spectrometer (BRUKER Tensor-37) was used to examine the surface-functionalization of the new membranes in the range of 4000–400  $\text{cm}^{-1}$ . A diamond prism was used as the waveguide and membrane holder. The membrane samples were dried at 40 °C/ overnight before analysis. The following abbreviations were used to specify the spectral bands: vs (very strong), s (strong), m (medium), w (weak), very weak (vw), sh (shoulder) and br (broad).

### 2.5.2. Morphological survey of the membranes

The cross-sectional and surface morphologies of the neat membrane and modified membranes were compared on the basis of scanning electron microscopy (SEM) micrographs. These SEM samples were prepared by breaking the membranes under liquid  $\text{N}_2$  to produce a generally consistent and clean cut. Then, the membranes were spin-coated with thin film of gold. Thereafter, the membrane samples were mounted on brass plates. Cross-sectional micrographs for our membranes were picked-up by an ESEM Quanta 400 FEG SEM equipped with a secondary electron detector (SED) and operated at 20 keV.

### 2.5.3. Hydrophilicity, water swelling (uptake) and contact angles of the membrane surface

Hydrophilicity of our new membranes was estimated by measuring the water contact angle (CA) using a steady contact angle measuring equipment (HHU, Düsseldorf, Germany). A schematic diagram of the measurement of CA of our membranes is depicted in Fig. S1. Multiple CA values have been measured and the average value was calculated with standard deviation.

The pH dependent swelling or water uptake features of the MMMs were examined following the procedure reported earlier in the previous work [30]. Briefly, a pre-weighed and ultra-dry membrane sample of weight  $W_d$  and 1  $\text{cm}^2$  area was immersed in phosphate buffer solutions with different pH values of 3, 5, 7, 9 and 11 for 24 h. Afterwards, the wet membrane was removed from the solution and the excess water on the outer surface of membrane was discarded using a blotting paper. Thereafter, the MMM sample was re-weighed as ( $W_w$ ) and the percentage of swelling or water uptake was calculated using equation (1):

$$\% \text{ Swelling (water uptake)} = \left( \frac{W_w - W_d}{W_d} \right) \times 100 \quad (1)$$

### 2.5.4. Membranes porosity

A QUANTACHROME POREMASTER 60-GT was used for pore analysis by means of mercury porosimetry. The basis of this method is the so-called Washburn equation, which used for a non-wettable liquid (mercury) represents the dependence of the pressure (to be filled) or empty (extrusion) pore diameter of the applied pressure. With the POREMASTER 60-GT, filling of the measuring cells before the actual measurement is done in a horizontal position: This prevents a static pressure of the heavy mercury (density approx.  $13.5 \text{ g/cm}^3$ ) on the sample and an undetected filling of large pores. Two strips of approximately  $8 \times 30 \text{ mm}$  were used for the measurement per sample. The samples were not previously dried but measured in the initial state. The results of the measurements are shown as an intruded volume versus pressure or versus pore diameter.

## 2.6. Membrane Performance Characterization

### 2.6.1. Pure water permeation ultrafiltration experiments

The PWF of the MMM with an effective area of  $5 \text{ cm}^2$  was carried out using a cross-flow ultrafiltration laboratory apparatus (Fig. 2). The membrane was soaked in milli-Q water for 24 h before running the water permeation experiment.

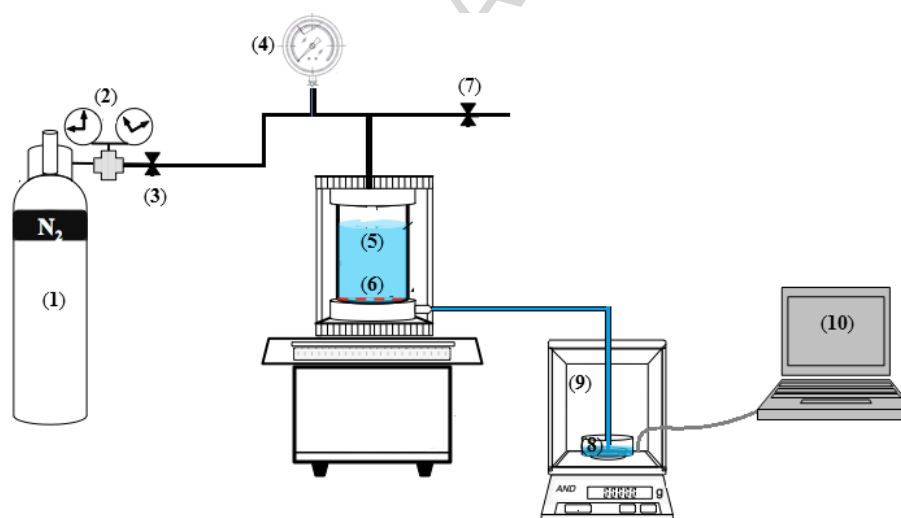


**Fig.2:** Schematic diagram of the permeation experimental apparatus: (1)  $\text{N}_2$  gas; (2,4) pressure gauges; (3,7) valves; (5) feed tank; (6) membrane; (8) permeate reservoir; (9) electronic balance; (10) computer.

Afterwards, membrane was compacted at a trans-membrane-pressure (TMP) of 0.10 MPa for 30 min. Then, the time dependent PWF was measured at 0.3 MPa. The permeate samples were collected after 15 min of exposure of a membrane to the target TMP at  $26 \text{ }^\circ\text{C}$  and the amount of water permeate was weighted every 10 min. Then the PWF ( $J_w$ ) was calculated using equation (2):

$$J_w = \left( \frac{Q}{A\Delta t} \right) \quad (2)$$

Where  $Q$  = volume of pure water collected during time  $\Delta t$  (h) using a MMM of area  $A$  ( $m^2$ ) and  $J_w$  is expressed in  $L/m^2h$ .

### 2.6.2. Antifouling assessment

Bovine serum albumin (BSA) has been chosen as a model fouling-induced protein to examine the antifouling efficacy of new modified MMMs [31].

#### BSA ultrafiltration experiments

The membrane fouling propensity was evaluated during the ultrafiltration of BSA aqueous solution. Initially, all MMMs were compacted at 0.1 MPa for 30 min. Then, the TMP was raised to 0.3 MPa. After 90 min of a water flow, the steady state water flux was calculated and assigned as  $J_{w1}$  ( $L/m^2h$ ). Afterwards, the pure water was replaced by a BSA aqueous solution (0.8 g/L). BSA flux at the end of the next 90 min was calculated and assigned as  $J_{BSA}$  ( $L/m^2h$ ). BSA rejection ( $R\%$ ) was estimated by UV-Vis spectroscopy at a wavelength of 280 nm and calculated using equation (3):

$$R\% = \left( 1 - \frac{C_{BSA}^{Permeate}}{C_{BSA}^{Feed}} \right) \times 100 \quad (3)$$

Here,  $C_{BSA}^{Permeate}$  (mg/mL) and  $C_{BSA}^{Feed}$  (mg/mL) represent the concentration of BSA solution in permeate and feed, respectively. After BSA UF experiment, the MMM was flushed with milli-Q water for 15 min before measuring the steady state PWF again a 90 min and assigned as  $J_{w2}$  ( $L/m^2h$ ). Finally, the membrane antifouling efficacy was calculated as a flux recovery ratio (FRR) using equation (4):

$$FRR\% = \left( \frac{J_{w2}}{J_{w1}} \right) \times 100 \quad (4)$$

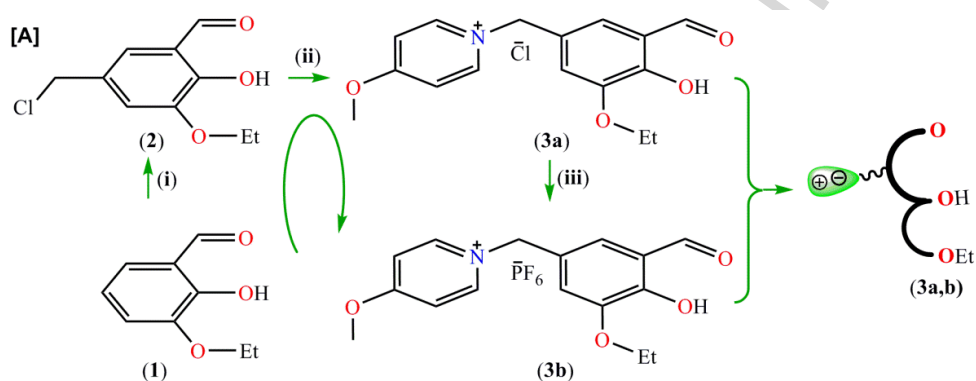
Eventually, the antifouling capacities of these MMMs can be predicted from several ratios including FRR (%) and total fouling  $R_t$  ( $R_t = 1 - J_{BSA}/J_{w1}$ ), reversible fouling  $F_r$  ( $F_r = (J_{w2} - J_{BSA})/J_{w1}$ ) and irreversible fouling  $F_{ir}$  ( $F_{ir} = (J_{w1} - J_{w2})/J_{w1}$ ) [32].

## 3. Results and Discussion

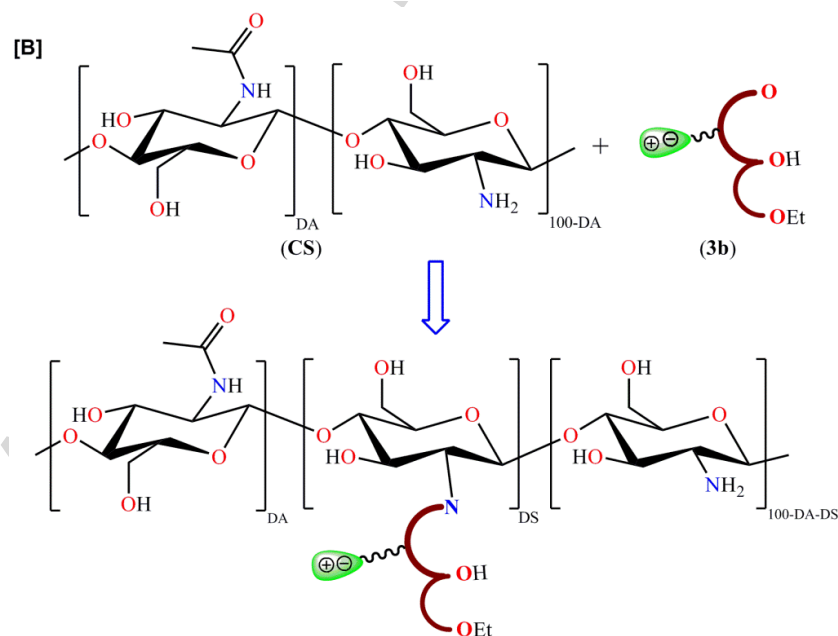
### 3.1. Chemistry

Multiple chemical strategies (chloromethylation, quaternization, anion metathesis and Schiff-base condensation, as well) (Scheme 1) were utilized for the surface modification of a natural biopolymer chitosan (CS). We have prepared a new hydrophilic antifouling agent,

poly-methoxypyridinium ethoxysalicylidene grafted-CS (**PILCSB**), from methoxypyridinium-ethoxysalicylaldehyde hexafluorophosphate (**3b**), which was in turn obtained from 3-ethoxysalicylaldehyde (**1**) according to Scheme 1. Chloromethylation of **1** was carried out with hydrochloric acid and polyoxymethylene (POM) as a formaldehyde precursor in a catalytic zinc chloride environment under aqueous biphasic conditions. The obtained chloromethylaldehyde (**2**) was then effectively aminated with 4-methoxypyridine (4-MeOPy) to yield methoxypyridinium-based salicylaldehyde chloride (**3a**). Subsequent chloride-hexafluorophosphate anion metathesis of **3a** using hexafluorophosphoric acid yielded the corresponding hexafluorophosphate salt (**3b**).



- (i) Chloromethylation:  $(\text{CH}_2\text{O})_n$ ,  $\text{ZnCl}_2$ ,  $\text{HCl}_{\text{aq}}$ ,  $\text{HCl}_{\text{g}}$ , stir, r.t. (ii) Quaternization: 4-MeOPy, toluene, stir, 80 °C,  $\text{N}_2$ .  
 (iii) Anion metathesis: 60%  $\text{HPF}_6$ , milli-Q  $\text{H}_2\text{O}$ , stir, 5 °C



**Scheme 1** Schematic diagram for different chemical strategies used in the synthesis of poly-methoxypyridinium ethoxysalicylidene brushes-based CS (**PILCSB**).

Eventually, the desired poly-methoxypyridinium ethoxysalicylidene brushes-based CS (**PILCSB**), was obtained by a simple efficient Schiff base condensation of ionic

salicylaldehyde hexafluorophosphate (**3b**) with the natural biopolymer, CS. This new antifoulant was isolated in excellent overall yield of 97.9%, structurally characterized based upon elemental analysis, ATR-FTIR, NMR ( $^1\text{H}$ ,  $^{13}\text{C}$ ,  $^{19}\text{F}$ ,  $^{31}\text{P}$ ) and morphologically examined by SEM micrographs.

### 3.2. Structural characterizations of CS and PILCSB

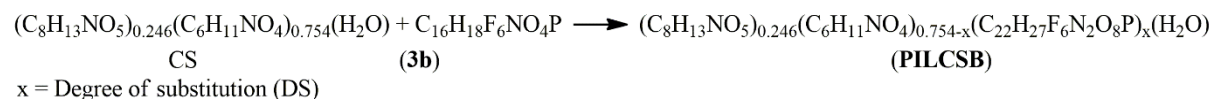
#### 3.2.1. Structural characterizations of CS

Based on the elemental and spectral data for CS, the degree of deacetylation (DDA) was found to be ~75.4% (See ESI†). Thus the plausible building unit of CS is a copolymer from GlcNHAc and GlcNH<sub>2</sub> kept at *ca.* 1:3 molar ratio, *i.e.*, (GlcNHAc)<sub>0.246</sub>(GlcNH<sub>2</sub>)<sub>0.754</sub> or (C<sub>8</sub>H<sub>13</sub>NO<sub>5</sub>)<sub>0.246</sub>(C<sub>6</sub>H<sub>11</sub>NO<sub>4</sub>)<sub>0.754</sub>·H<sub>2</sub>O.

#### 3.2.2. Structural characterizations of PILCSB

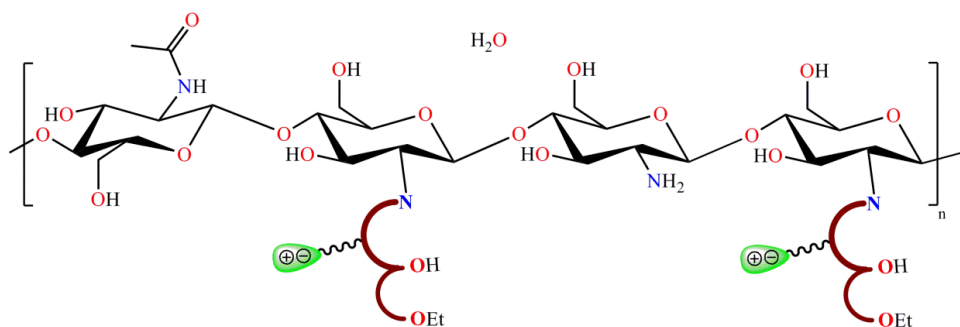
##### Microanalytical data and degree of substitution DS (Iminization) for PILCSB

During the synthesis protocol of PILCSB, the experimental conditions were optimized for achieving almost complete conversion of CS into the corresponding PILCSB. Thus, the experimental yield of **PILCSB** may be plausibly used for calculation of its degree of substitution (DS) (iminization) according to the reaction depicted in Scheme 2;



**Scheme 2** Schematic conversion of CS into the corresponding Schiff base (**PILCSB**), antifoulant.

Here, Schiff base condensation of (1.00 g) CS with **3b** yielded 2.13 g of **PILCSB** which means a 113% massive increase in the weight of CS and the MW of the building block of **PILCSB**, accordingly. Thus, the MW of the resulting **PILCSB** is higher than that of CS (MW<sub>CS</sub> = 189.51 g/mol) by 113%, *i.e.* MW<sub>4b</sub> = 403.84 g/mol which represents the MW of the monomeric building block suggested for **PILCSB** in Scheme 2, (C<sub>8</sub>H<sub>13</sub>NO<sub>5</sub>)<sub>0.246</sub>(C<sub>6</sub>H<sub>11</sub>NO<sub>4</sub>)<sub>0.754-x</sub>(C<sub>22</sub>H<sub>27</sub>F<sub>6</sub>N<sub>2</sub>O<sub>8</sub>P)<sub>x</sub>(H<sub>2</sub>O). Solving this formula gives the value of DS as 49.7% which is in good agreement with the results obtained from CHN analysis for **PILCSB**. Anal. Calcd for (C<sub>8</sub>H<sub>13</sub>NO<sub>5</sub>)<sub>0.246</sub>(C<sub>6</sub>H<sub>11</sub>NO<sub>4</sub>)<sub>0.257</sub>(C<sub>22</sub>H<sub>27</sub>F<sub>6</sub>N<sub>2</sub>O<sub>8</sub>P)<sub>0.497</sub>(H<sub>2</sub>O) (MW = 403.85 g/mol): 42.96; H, 5.35; N, 5.19. Found for **PILCSB** (DS = 49.7%) C, 42.85; H, 5.42; N, 5.03. So, on the basis of elemental analyses, the suggested structure for the desired antifoulant, poly-methoxypyridinium ethoxy-salicylidene brushes-based CS (**PILCSB**), is depicted in Scheme 3.



**Scheme 3** Suggested structural formula for **PILCSB**.

### FTIR

Changes in the ATR-FTIR signatures of **PILCSB** in comparison to the parent CS (Fig. S2, ESI) demonstrate the successful covalent grafting of the hydrophilic poly-methoxypyridinium ethoxysalicylidene brushes on the surface of CS fibers. Where, the absorption at *ca.*  $3438\text{ cm}^{-1}$  along with two maxima at  $1644\text{ cm}^{-1}$ , characteristic for superimposed C=O (amide I) and azomethine (H-C=N) stretching vibrations, and  $1277\text{ cm}^{-1}$ , characteristic for aryl-O vibration, can be attributed to the overlapping of phenolic O-H and amide N-H stretching modes. Pertinacity of  $\nu_{\text{NH}_2}$  peak to participate in the spectrum of **PILCSB**, however, with a very feeble extent compared to that of CS, confirms the predominance poly-methoxypyridinium ethoxysalicylidene brushes on the CS surface, *via* partial Schiff base condensation, with minor contribution of neat glucosamine (GlcNH<sub>2</sub>) units. Three predominant peaks (C=N stretching:  $1526\text{ cm}^{-1}$ ; PF<sub>6</sub><sup>-</sup> stretching:  $840\text{ cm}^{-1}$  and bending:  $740\text{ cm}^{-1}$ ) are assignable to the methoxypyridinium terminals.

### NMR spectroscopy

Consistent with a successful surface modification of CS with poly-methoxypyridinium ethoxysalicylidene brushes is the appearance of novel signals in the <sup>1</sup>H NMR spectrum of **PILCSB** compared to the one of CS such as the highly deshielded peaks at  $\delta = 12.28$  and  $8.91$  ppm arising from phenolic OH involved in an intramolecularly H-bonded environment [33] and aldimine protons, respectively. A set of multiplets in the range of  $8.36$ – $7.24$  ppm is due to the resonance of aromatic protons. The <sup>13</sup>C NMR spectrum for **PILCSB** offers further evidence for the successful chemical anchoring of poly-methoxypyridinium ethoxysalicylidene compartments to the chitosan skeleton as revealed from the observation of two low-field resonance signals at  $166$  and  $158$  ppm attributed to phenolic and azomethinic carbons, respectively. The hexafluorophosphate ion was authenticated by a septet signal centered at *ca.*  $-138$  ppm with  $^2J_{\text{PF}} = 711.18$  Hz coupled with a doublet signal centered at *ca.* -

65.5 ppm with  $^1J_{\text{PF}} = 711.24$  Hz in their  $^{31}\text{P}/^{19}\text{F}$  NMR spectra which are characteristic for  $\text{PF}_6^-$  counter anions.

### 3.2.3. Morphological and topographical characterizations of **PILCSB**

The morphology of the texture for the **PILCSB** was investigated from SEM micrographs (see Fig. S3, ESI), which revealed a significant difference between the surface morphology of **PILCSB** and CS. Where CS exhibits a flat surface with a smooth and dense texture while **PILCSB** has a rough sponge-like texture. This could be attributed to the expected interactions between CS matrix and **PILCSB** through H-bonding and imine linkages leading to the formation of many hydrophilic sites at the surface with cross-sectional pores and micro voids network.

### 3.3. Morphological and textural properties of TNPs

The morphology of TNPs prepared starting from  $\text{TiCl}_4$  by a solution-based method was probed using SEM analysis (Fig. 3, Fig S4). SEM image revealed that most of the TNPs were spherical with a regular diameter ranging from 39 nm to 57 nm.

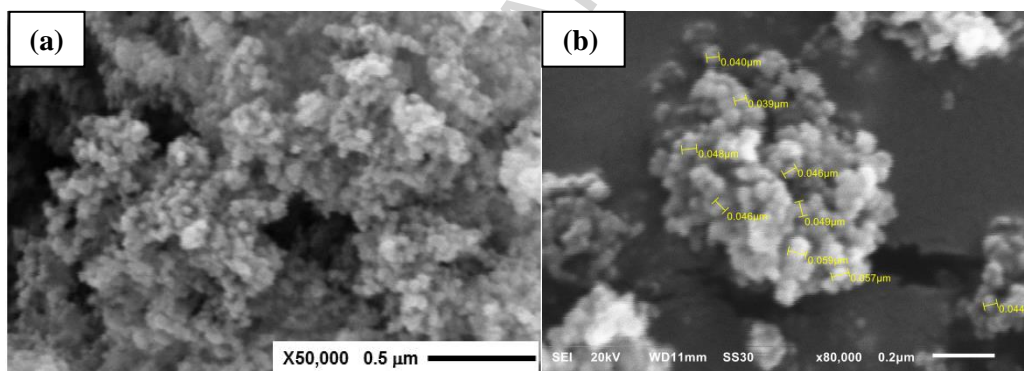


**Fig. 3** SEM micrograph of TNPs; (a) General view, (b) an approximate grain-size range (in  $\mu\text{m}$ ) of TNPs.

The phase purity of TNPs was estimated from the XRD diffractogram (Fig. 4a). All observed major peaks are well recorded to the TNPs in an anatase phase as indicated by the standard (JCPDS card No. 21-1272).

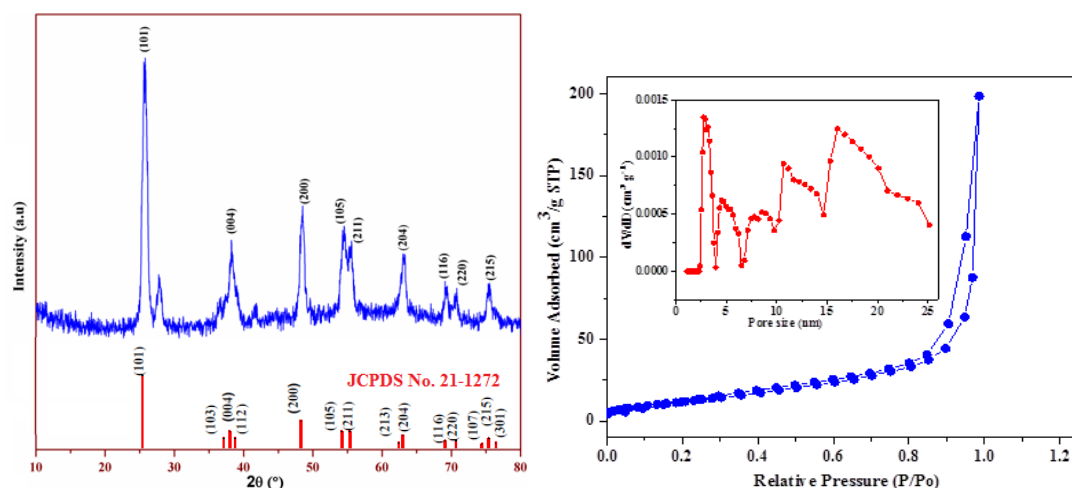


**Fig. 4** (a) X-ray diffraction patterns (Cu-K $\alpha$  radiation) of TNPs. (b) N<sub>2</sub> adsorption–desorption isotherms along with the corresponding pore size distributions (inset) of the TNPs at 77 K.

The specific surface areas and pore size distributions of the as-synthesized TNPs was established using nitrogen adsorption–desorption isotherm (Fig. 4b) which reflect a type IV isotherm with H2 hysteresis loop according to Brunauer–Deming–Deming–Teller (BDDT) classification [34]. This hysteresis loop implies that the TNPs have mesoporous structure, with specific surface area of 94 m<sup>2</sup>g<sup>-1</sup> and the pore size distribution curve (inset in Fig. 4b) shows a wide range of pore size from 3.3 to 25 nm with a maximum population of ~3.3 nm.

### 3.4. Membranes characterization

#### 3.4.1. ATR-FTIR

ATR-FTIR spectroscopy can provide information about the surface and near-surface composition of the membranes. Where the presence of CS or new antifoulant (**PILCSB**) onto the outer surface of PSU was evident by ATR-FTIR spectroscopy. In comparison to the FTIR spectra of pure PSU and **PILCSB**, PSU@**PILCSB**@(PEG)@(TNPs) (MMM4, MMM5, MMM6) membranes exhibit collective infrared spectral signatures of their woven components, confirming successful fabrication of MMMs. The ATR-FTIR spectra of the new membranes (Fig. 5) revealed common features represented by the characteristic peaks around 3420 cm<sup>-1</sup> corresponding to the amide N–H and alcoholic/ phenolic OH stretches of **PILCSB**. The amide N-H peaks is in line with the characteristic for amide C=O peak around 1670 cm<sup>-1</sup>. The OH peak is in line with the Ar–O vibration mode around 1275 cm<sup>-1</sup>. The vibration peaks characteristic for PSU are seen around 1294 and 1150 cm<sup>-1</sup>, assignable to asymmetric and symmetric stretching vibrations, respectively, of the O=S=O group, along with a peak observed around 1240 cm<sup>-1</sup> attributable for the C–O–C vibration.

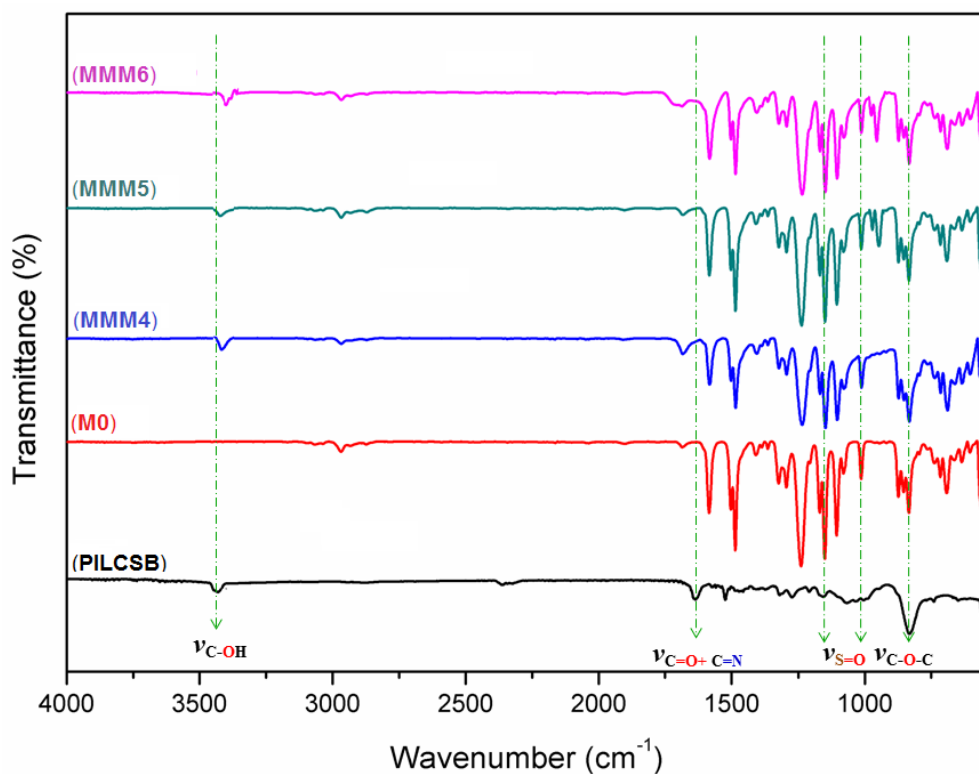


**Fig. 5** ATR-FTIR patterns for comparison of the FTIR signatures of MMMs with parents **PILCSB** and PSU.

### 3.4.2. Morphology of the membranes

The overall thicknesses of the newly fabricated MMMs were in the range of 80–110  $\mu\text{m}$ . The surface and cross-section morphologies of these new MMMs were inspected by SEM. The cross-sectional SEM micrographs (Fig. 6) revealed that all membranes exhibited asymmetric porous structure of a dense skin layer and a highly porous sub-layer containing sponge-like structure (for CS-based MMMs) or macrovoid-type structure (in case of **PILCSB**-based MMMs). These changes in membrane morphologies could be ascribed to the replacement of CS with a poly-methoxy pyridinium ethoxysalicylidene brush-based CS, a violent hydrophilic antifouling additive, which enhances the hydrophilicity and subsequently the affinity of the PSU@**PILCSB**@PEG@(TNPs) (MMM6) casting composite which already dissolved in NMP to the non-solvent (water) coagulation bath compared to PSU@CS@PEG@(TNPs) (MMM3) which reduce the mutual diffusivity between casting solvent (NMP) and non-solvent (water). This prolonged mutual diffusion allowed longer phase inversion time along with lower segregation rate of **PILCSB** from the bulk casting solution up to the NMP-water interface and self-induced pore growth, as well. Moreover, the hydrophilic nature of the TNPs facilitated the mass transfer between the NMP and the water during phase inversion resulting in the development of longer macrovoids and subsequently

the enhancement of overall membrane porosity [35].

The successful formulation of TNPs into the membrane matrix was proved by EDX results (mapping and spectra) as depicted in Fig. S6 (ESI†). All new MMMs are typical UF membranes with micrometer-scale pores upon the surface layer and micron-sized macrovoids embedded across the membrane network.

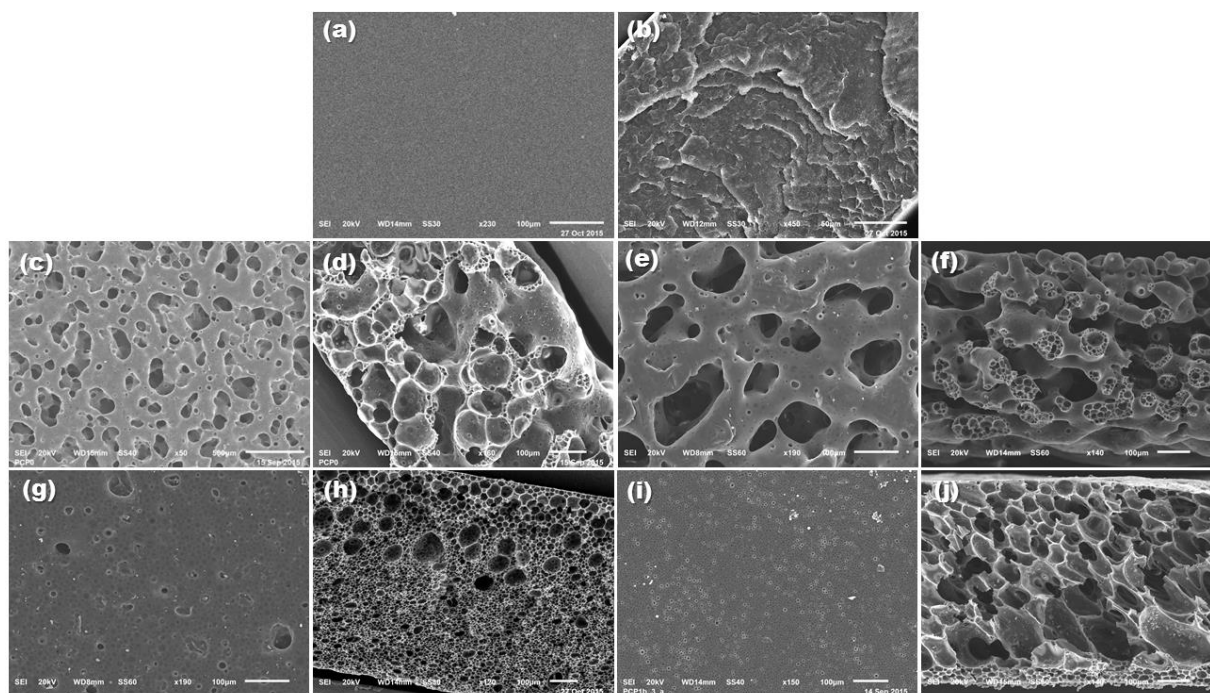


**Fig. 6** Surface and cross-sectional SEM micrographs of: (a, b) M0, (c, d) MMM2, (e, f) MMM3, (g, h) MMM4, (i, j) MMM6.

### 3.4.3. Porosity

The pore size distribution (PSD) plot for MMM2 and MMM5, as representative examples of MMMs is depicted in Fig. 7. As shown in in this figure, MMM2 possess "channels and pores" where the surface shows many channel windows 10-100  $\mu\text{m}$ . Inside of the walls between channels, there are spherical pores with a hierarchical size distribution ranging from internal smaller pores with  $\sim 10$   $\mu\text{m}$  diameter to external larger pores of  $\sim 100$   $\mu\text{m}$  diameter. The MMM5 texture exhibited asymmetric pore distribution with large pores of 50-100  $\mu\text{m}$  in the center and small pores of 10-20  $\mu\text{m}$  to the outside of the membrane. Moreover, the surfaces of MMM2 and MMM5 show some pore windows 5-10  $\mu\text{m}$ , while, the untreated membrane (M0) shows slightly rough cross-section but no pores as revealed from its SEM micrograph (*cf.* Fig. 6)

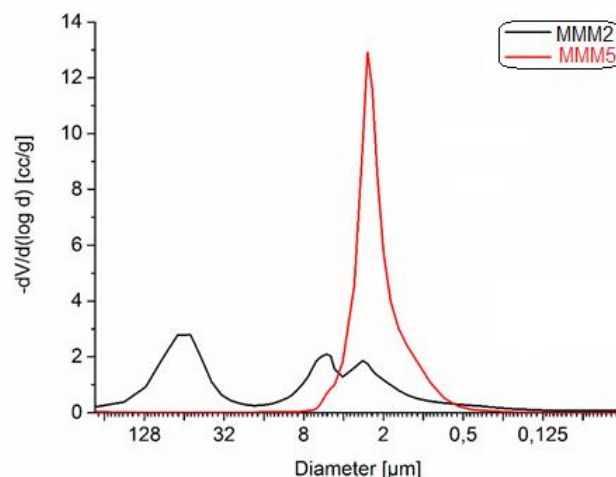


**Fig. 7** Pore size distribution (PSD) curve which is calculated from the normalized volume curve by differentiation for MMM2 and MMM5 (representative examples of MMMs).

### 3.5. Membranes performance

#### 3.5.1. Water uptake (membrane swelling) and contact angle measurement

Water uptake, swelling ratio and contact angle values of new MMM surfaces were assessed to evaluate their hydrophilicity/ hydrophobicity features. As revealed from Fig. 8a, the water uptake and swelling ratio values of **PILCSB**-blended MMMs were higher than those of the neat PSU membrane and CS-based PSU membranes because of the existence of poly-methoxypyridinium ethoxysalicylidene brushes on the active layer of membrane, as revealed from EDX (*cf.* Fig. S5, ESI<sup>†</sup>), which offer multiple active H-bonding sites for interaction with water. Noteworthy, water uptake performance was changed in a pH-dependence profile with maximum uptake under acidic conditions (pH=4) due to protonation of the GlcNH<sub>2</sub> fragments of CS. At pH = 4, a maximum water uptake of 83.46% was achieved for PSU@**PILCSB**@PEG@TNPs (MMM6). Thus, water uptake in membranes depends on the content of hydrophilic TNPs. Noteworthy, the addition of TNPs didn't significantly change the hydrophilicity of the PSU membrane as revealed from water contact angle measurements depicted in Fig. 8b, however, **PILCSB** brushes coated TNPs was greatly enhanced the MMM6 hydrophilicity.

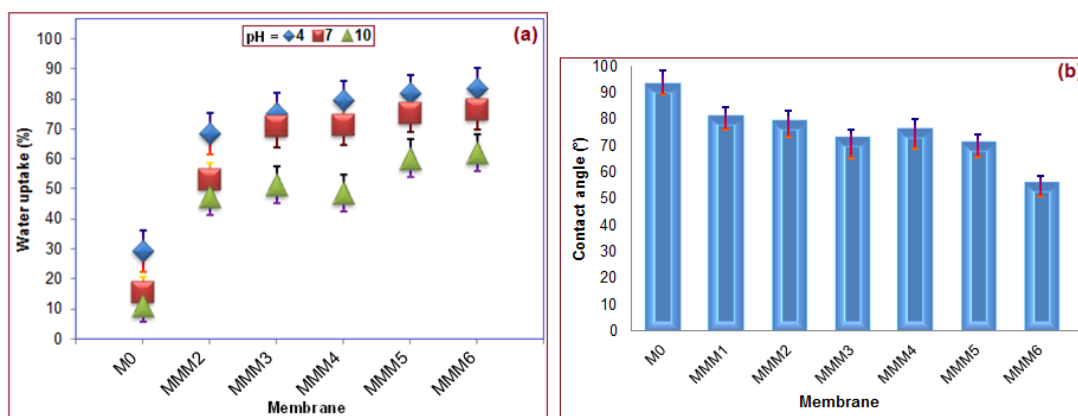


**Fig. 8** (a) pH dependent water uptake of MMMs in comparison with neat PSU membrane M0. (b) Contact angle of MMMs compared to neat PSU membrane.

As shown in Fig. 8b, all woven membranes had water contact angles lower than  $90^\circ$ , indicating that the highly hydrophobic properties of the parent PSU (water contact angle =  $93.48^\circ$ ) were decreased to be somewhat more hydrophilic as a result of its surface refinement with hydrophilic architectures (i.e., CS or **PILCSB**, PEG, TNPs). The membranes MMM4-6 modified with **PILCSB**, exhibit somewhat lower water contact angles compared to those modified with CS (MMM1-3) because the multiple hydrophilic fragments in the polymethoxypyridinium ethoxysalicylidene brushes of **PILCSB** impart higher hydrophilicity than CS. Moreover, the entrapment of TNPs on the matrix of the membrane led to an enhancement of membrane hydrophilicity as revealed from the observed water contact angle ( $57.35^\circ$ ) for MMM6.

### 3.5.2. Permeation properties

The permeation performance of the pristine PSU membrane (M0) and the MMMs were determined by pure water (PWF) and BSA filtration experiments. From the PWF and BSA rejection data for the virgin PSU membrane and the MMMs presented in Table 2, it is noticeable that the virgin membrane M0 manifested an extremely low water flux of  $60 \text{ L/m}^2 \text{ h}$  coupled with the elevated level of BSA rejection, 89.95%, under an operation pressure of 0.3 MPa, which is in accordance with its higher hydrophobicity. The water permeability of the PSU-based composite MMMs was distinctly enhanced by integration of the hydrophilic biopolymer CS or the amphiphilic copolymer (**PILCSB**), pore stabilizing agents (PEG) and  $\text{TiO}_2$ -NPs into the matrix of the membrane. Particularly, the PWF of MMM6 is  $158.10 \text{ L/m}^2 \text{ h}$  ( $\sim 2.7$  times higher than that of the native PSU membrane), moreover, it has the maximum BSA rejection, 36%.

**Table 2.** PWF ( $J_{w1}$ ) and BSA rejections of the membranes <sup>a</sup>

Membrane ID	composition	PWF (L/m <sup>2</sup> h)	BSA rejection (%)
M0	pure PSU	69	90
MMM1	PSU@CS	76	68
MMM2	PSU@CS@PEG	95	53
MMM3	PSU@CS@PEG@TNPs	99	52
MMM4	PSU@ <b>PILCSB</b>	129	43
MMM5	PSU@ <b>PILCSB</b> @PEG	144	37
MMM6	PSU@ <b>PILCSB</b> @PEG@TNPs	158	36

<sup>a</sup> PWF = pure water flux; BSA = Bovine serum albumin.

It is recognized that the water permeability of the membrane is governed by its physical (hydrophilicity/ hydrophobicity), geometrical (porous network, pore size and roughness) and chemical (liquid-solid interactions) parameters [36]. In this context, enhancing the hydrophilicity of the surface of PSU membrane by blending it with a hydrophilic additive (CS or **PILCSB**) will reduce the membrane affinity for physisorption of organic contaminants (such BSA). A hydrophilic additive will also promote the hydrophilic pore-water interaction within the porous framework and, thus, improve the water mass transport. The BSA rejection was dramatically decreased as the hydrophilic additives (CS, **PILCSB**, PEG and TNPs) were incorporated into the PSU membrane as presented in Table 2. Specifically, MMM6 which exhibits promising performance because of it combines **PILCSB** with polar ionizable moieties that induce surface charges which promote wettability of the membrane while diminishing BSA-membrane interaction.

### 3.5.3. Antifouling properties of membranes.

A consecutive water-BSA-water permeation experiment was used to assess the antifouling performance of the composite membranes (MMMs) in comparison with the virgin PSU membrane (M0). As shown in Fig. 9, the permeation flux for the M0 dropped dramatically when the pure water permeation was followed with the fouling-inducing model BSA solution. This drop may be attributed to the hydrophobic surface which promotes membrane fouling *via* hydrophobic (M0-BSA) interaction. On the other hand, the MMMs exhibited lower flux decline than the neat PSU membrane M0 suggesting that the composite membranes have lower fouling propensity than the pure PSU membrane. This could be assigned to an increase of the membrane surface hydrophilicity by blending with hydrophilic fillers which reduce its fouling propensity and diminish the flux declining degree, accordingly. Noteworthy, the composite membranes (MMMs) exhibited a higher relative

fluxes recovery than M0 after simple hydraulic cleaning as revealed from the water permeation following BSA filtration (section (III) in Fig. 9). These results suggest reversibility of the fouling for the MMMs which is in good agreement with their enhanced surface hydrophilicity.

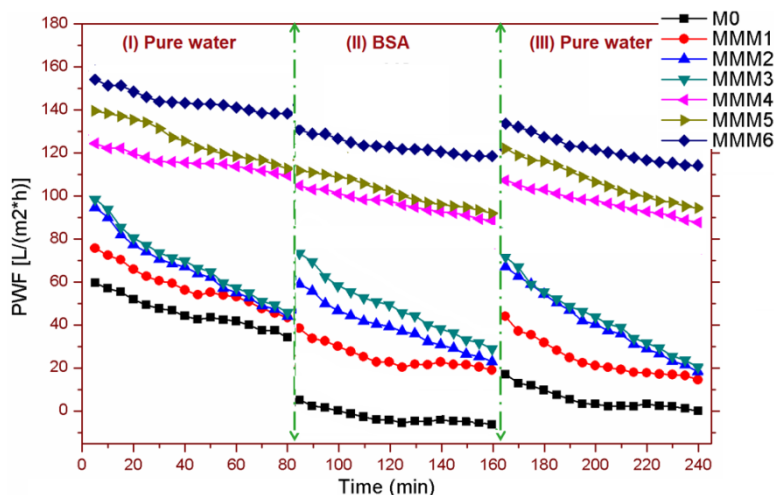


**Fig. 9.** Flux decline and recovery results for the as-fabricated MMMs. This permeation experiment contains three phases: (I) pure water permeation, Experimental conditions: Initially, a 5 cm<sup>2</sup> membrane was compacted at 0.10 MPa, a trans-membrane-pressures (TMP), for 30 min. Then, the time dependent pure water flux (PWF) was measured at 0.3 MPa. The permeate sample collection was started after 15 min of exposure to target TMP at 26 °C and the permeate was weighted every 10 min, and operation period of 90 min. (II) BSA solution (model foulant) filtration, and (III) pure water permeation after water flushing.

Reversible fouling ( $F_r$ ): arises from reversible adsorption/ deposition of a foulant protein (BSA) and can be easily removed by simple water flushing. Irreversible fouling ( $F_{ir}$ ) is due to the irreversible adsorption of a protein (BSA) and can only be eliminated by chemical treatment. Thereafter, quantitative assessment of the antifouling capacities of these membranes have been addressed based upon several ratios including flux recovery ratio (FRR), total fouling ( $F_t$ ), reversible and irreversible fouling ( $F_r$ ,  $F_{ir}$ ) as depicted in Fig. 10. It is clear from Fig. 10 that the FRR(%) values for the MMMs (67-89%) are much higher than those of nascent PSU (M0), confirming the lower fouling propensity of the MMMs [37]. This indicated that the MMMs could keep a higher water flux even after a BSA UF process [38]. Collected  $F_t$ ,  $F_r$  and  $F_{ir}$  values for the MMMs provide further evidence for their promotion of antifouling performance as revealed from Fig. 10, where these values are greatly reduced by blending of PSU with the antifoulants (**PILCSB** and **TNPs**) assignable to the increased

hydrophilicity of MMMs.

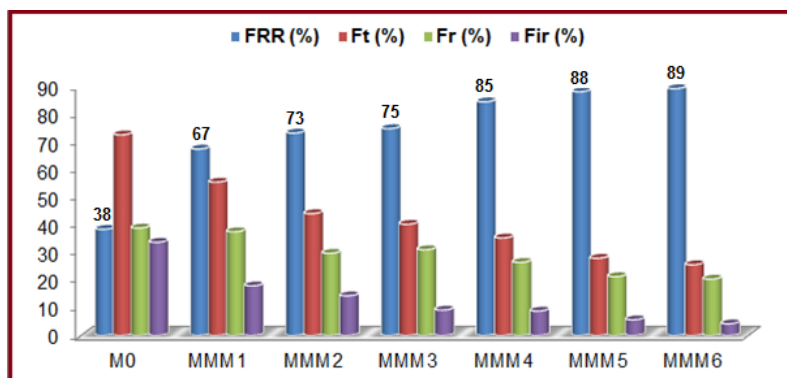


**Fig. 10.** A summary of total fouling ( $F_t$ ), reversible fouling ( $F_r$ ), irreversible fouling ( $F_{ir}$ ), and flux recovery ratio (FRR) for neat PSU (M0) and composite MMMs with CS, **PILCSB** and TNPs.

Consequently, the hydrophilic fillers (**PILCSB** and TNPs) are believed to form a hydration barrier that diminished the fouling model (BSA) adsorption.

#### 4. Conclusion

In our work, PSU UF-membrane was physically modified with chitosan (CS) and poly-ionic liquid-grafted chitosan Schiff base (**PILCSB**) and TNPs in presence of pore-stabilizing agent, PEG. The effect of these additives on the morphology, porosities features, water flux, protein rejections and antifouling performances of the modified membranes (MMMs) was investigated. The results revealed that incorporation of all additives into a mixed matrix membrane **MMM6** (PSU@**PILCSB**@PEG@TNPs) was significantly enhanced membrane texture and permeation performance with and improved pure water flux by 2.5 fold in comparison to the neat PSU membrane (M0). Moreover **MMM6** exhibited the highest resistance to biofouling for the UF applications.

#### ACKNOWLEDGMENT

The authors gratefully acknowledge the financial support of the Federal German Ministry of Education and Research (BMBF) in the project Optimat under grant no. 03SF0492C

#### APPENDIX A. SUPPLEMENTARY DATA

Supplementary data (experimental and spectral data) associated with this article are available with the article through the journal Web site, at doi:

## REFERENCES

- 
- [1] Human Development Report, Chapter 4, United Nations Development Programme (UNDP) (2006).
- [2] Urban Urgency, Water Caucus Summary, World Water Council (WWC), Marseille, France (2007).
- [3] M. Mulder, Basic Principles of Membrane Technology, Kluwer Academic Publishers, London (1996).
- [4] (a) Y. H. Cho, H. W. Kim, S. Y. Nam, H. B. Park, Fouling-tolerant polysulfone–poly(ethylene oxide) random copolymer ultrafiltration membranes, *J. Membr. Sci.*, 37 (2011) 296-306;  
(b) N. Nady, M. C. R. Franssen, H. Zuilhof, M. S. M. Eldin, R. Boom, K. Schroën, Modification methods for poly(arylsulfone) membranes: a mini-review focusing on surface modification, *Desalination*, 275 (2011) 1-9.
- [5] K. J. Lee, J. Y. Jae, Y. S. Kang, J. Won, Y. Dai, G. P. Robertson, M. D. Guiver, Gas transport and dynamic mechanical behavior in modified polysulfones with trimethylsilyl groups: effect of degree of substitution, *J. Membr. Sci.*, 223 (2003) 1-10.
- [6] Y. Liu, Shuling Zhang, G. Wang, The preparation of antifouling ultrafiltration membrane by surface grafting zwitterionic polymer onto poly (arylene ether sulfone) containing hydroxyl groups membrane, *Desalination*, 316 (2013) 127-136.
- [7] (a) J. Sikder, C. Pereira, S. Palchoudhury, K. Vohra, D. Basumatary, P. Pal, Synthesis and characterization of cellulose acetate-polysulfone blend microfiltration membrane for separation of microbial cells from lactic acid fermentation broth, *Desalination*, 249 (2009) 802-808;  
(b) N. K. Saha, M. Balakrishnan, M. Ulbricht, Fouling control in sugarcane juice ultrafiltration with surface modified polysulfone and polyethersulfone membranes, *Desalination*, 249 (2009) 1124-1131;  
(c) R. Kumar, A. M. Isloor, A. F. Ismail, S. A. Rashid, T. Matsuura, Polysulfone–Chitosan blend ultrafiltration membranes: preparation, characterization, permeation and antifouling properties. *RSC Adv.*, 3 (2013) 7855- 7861.
- [8] (a) Q. Shi, Y. L. Su, W. Zhao, C. Li, Y. H. Hu, Z. Y. Jiang, S. P. Zhu, Zwitterionic polyethersulfone ultrafiltration membrane with superior antifouling property, *J. Membr. Sci.*, 319 (2008) 271-278;  
(b) D. Rana, T. Matsuura, Surface modifications for antifouling membranes, *Chem. Rev.*, 110 (2010) 2448–2471;  
(c) J. A. Koehler, M. Ulbricht, G. Belfort, Intermolecular forces between a protein and a hydrophilic modified polysulfone film with relevance to filtration, *Langmuir*, 16 (2000) 10419-10427.
- 9 (a) Q. F. Zhang, S. B. Zhang, L. Dai, X. S. Chen, Novel zwitterionic poly(arylene ether sulfone) s

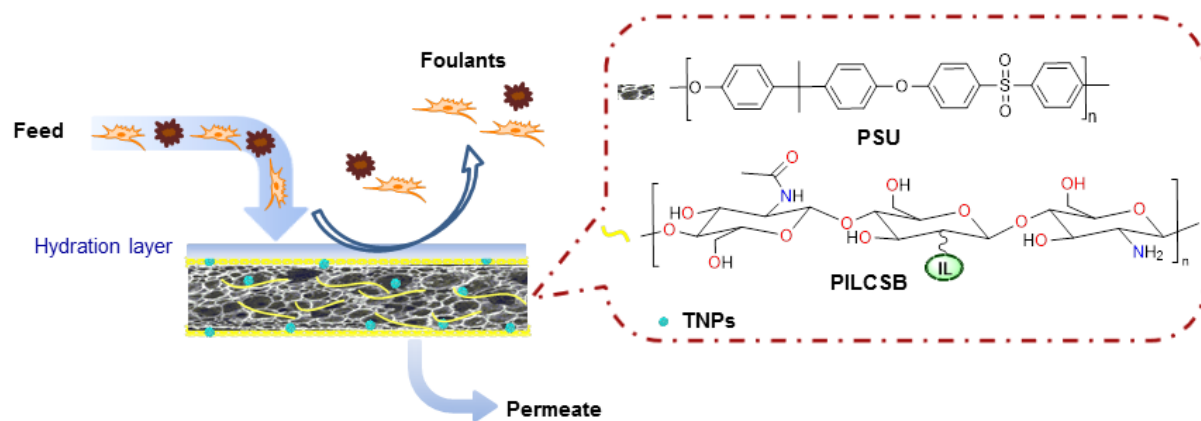
- as antifouling membrane material, *J. Membr. Sci.*, 349 (2010) 217-224;
- (b) Y. G. Dave, A. V. R. Reddy, Preparation, characterization, acid stability and organic fouling of poly(acrylonitrile-co-methacrylic acid) ultrafiltration membranes, *Desalination*, 282 (2011) 9-18;
- (c) M. P. Sun, Y. L. Su, C. X. Mu, Z. Y. Jiang, Improved antifouling property of PES ultrafiltration membranes using additive of silica-PVP nanocomposite, *Ind. Eng. Chem. Res.*, 49 (2010) 790-796.
- [10] (a) J. Jiang, L. Zhu, L. Zhu, H. Zhang, B. Zhu, Y. Xu, Antifouling and antimicrobial polymer membranes based on bioinspired polydopamine and strong hydrogen-bonded poly(N-vinyl pyrrolidone), *ACS Appl. Mater. Interfaces*, 5 (2013) 12895-12904;
- (b) H. Susanto, M. Ulbricht, Characteristics, performance and stability of polyethersulfone ultrafiltration membranes prepared by phase separation method using different macromolecular additives, *J. Membr. Sci.*, 327 (2009) 125-135;
- (c) H. Yu, Y. Cao, G. Kang, J. Liu, M. Li, Q. Yuan, Enhancing antifouling property of polysulfone ultrafiltration membrane by grafting zwitterionic copolymer via UV-initiated polymerization, *J. Membr. Sci.*, 342 (2009) 6-13.
- [11] (a) H. Dong, Y. Xu, Z. Yi, J. Shi, Modification of polysulfone membranes via surface-initiated atom transfer radical polymerization, *Appl. Surf. Sci.*, 255 (2009) 8860-8866;
- (b) D. S. Wavhal, E. R. Fisher, Hydrophilic modification of polyethersulfone membranes by low temperature plasma-induced graft polymerization, *J. Membr. Sci.*, 209 (2002) 255-269.
- [12] (a) D. Liu, D. Li, D. Du, X. Zhao, A. Qin, X. Li, C. He, Antifouling PVDF membrane with hydrophilic surface of terry pile-like structure, *J. Membr. Sci.*, 493 (2015) 243-251;
- (b) M. K. Sinha, M. K. Purkait, Preparation of fouling resistant PSF flat sheet UF membrane using amphiphilic polyurethane macromolecules, *Desalination*, 355 (2015) 155-168;
- (c) Q. Shi, J. Meng, R. Xu, X. Du, Y. Zhang, Synthesis of hydrophilic polysulfone membranes having antifouling and boron adsorption properties via blending with an amphiphilic graft glycopolymer, *J. Membr. Sci.*, 444 (2013) 50-59.
- [13] (a) F. Gao, G. Zhang, Q. Zhang, X. Zhan, F. Chen, Improved antifouling properties of Poly(Ether sulfone) membrane by incorporating the amphiphilic comb copolymer with mixed Poly(Ethylene glycol) and Poly(Dimethylsiloxane) brushes. *Ind. Eng. Chem. Res.*, 54 (2015) 8789-8800;
- (b) Q. Liu, A. A. Patel, L. Liu, Superhydrophilic and underwater superoleophobic poly-(sulfobetaine methacrylate)-Grafted glass fiber filters for oil–water separation. *ACS Appl. Mater. Interfaces*, 6 (2014) 8996-9003;
- (c) A. Venault, M. R. B. Ballard, Y. Liu, P. Aimar, Y. Chang, Hemocompatibility of PVDF/PS-b-PEGMA membranes prepared by LIPS process, *J. Membr. Sci.*, 477 (2015) 101-114.
- [14] (a) R. F. M. Elshaarawy, A. A. Refaee, E. A. El-Sawi, Pharmacological performance of novel

- poly-(ionic liquid)-grafted chitosan-N-salicylidene Schiff bases and their complexes, *Carbohydrate polymers*, 146 (2016) 376-387;
- (b) H. K. No, N. Y. Park, S. H. Lee, S. P. Meyers, Antibacterial activity of chitosans and chitosan oligomers with different molecular weights, *Int. J. Food Microbiol.*, 74 (2002) 65-72;
- (c) J. Rhoades, S. Roller, Antimicrobial actions of degraded and native chitosan against spoilage organisms in laboratory media and foods, *Appl. Envir. Microbio.*, 66 (1) (2000) 80-86;
- (d) B. K. Choi, K. Y. Kim, Y. J. Yoo, S. J. Oh, J. H. Choi, C. Y. Kim, In vitro antimicrobial activity of a chitooligosaccharide mixture against *Actinobacillus actinomycetemcomitans* and *Streptococcus mutans*, *Int. J. Antimicrob. Agents*, 18 (6) (2001) 553-557.
- [15] (a) R. F. M. Elshaarawy, F. H. A. Mustafa, A. Herbst, A. E. M. Farag, C. Janiak, Surface functionalization of chitosan isolated from shrimp shells, using salicylaldehyde ionic liquids in exploration for novel economic and ecofriendly antibiofoulants, *RSC Adv.*, 6 (2016) 20901-20915;
- (b) I. L. Roux, H. M. Krieg, C. A. Yeates, J. C. Breytenbach, *J. Membr. Sci.*, 248 (2005) 127-136.
- E. Bagheripour, A. R. Moghadassi, S. M. Hosseini, B. Van der Bruggen, F. Parvizian, Novel composite graphene oxide/chitosan nanoplates incorporated into PES based nanofiltration membrane: Chromium removal and antifouling enhancement, *J. Ind. Eng. Chem.*, 62 (2018) 311-320.
- [16] A. M. Motawie, K.F. Mahmoud, A. A. El-Sawy, H. M. Kamal, H. Hefni, H. A. Ibrahim, Preparation of chitosan from the shrimp shells and its application for pre-concentration of uranium after cross-linking with epichlorohydrin, *Egyptian J. Petroleum*, 23 (2014) 221-228.
- [17] Y. Mansourpanah, H. Soltani, K. Alizadeh, M. Tabatabaei, Enhancing the performance and antifouling properties of nanoporous PES membranes using microwave-assisted grafting of chitosan, *Desalination*, 322 (2013) 60-68.
- [18] (a) S. Zinadini, A. A. Zinatizadeh, M. Rahimi, V. Vatanpour, H. Zangeneh, M. Beygzadeh, Novel high flux antifouling nanofiltration membranes for dye removal containing carboxymethyl chitosan coated Fe<sub>3</sub>O<sub>4</sub> nanoparticles, *Desalination*, 349 (2014) 145-154;
- (b) J. Miao, G. Chen, C. Gao, C. Lin, D. Wang, M. Sun, Preparation and characterization of N,O-carboxymethyl chitosan (NOCC)/polysulfone (PS) composite nanofiltration membranes, *J. Membr. Sci.*, 280 (2006) 478-484;
- (c) J. Miao, G. Chen, C. Gao, S. Dong, Preparation and characterization of N,O-carboxymethyl chitosan/polysulfone composite nanofiltration membrane crosslinked with epichlorohydrin, *Desalination*, 233 (2008) 147-156.
- [19] (a) R. Kumar, A. M. Isloor, A. F. Ismail, T. Matsuura, Synthesis and characterization of novel water soluble derivative of Chitosan as an additive for polysulfone ultrafiltration membrane, *J. Membr. Sci.*, 440 (2013) 140-147;

- (b) Y. Chen, Y. Zhang, H. Zhang, J. Liu, C. Song, Biofouling control of halloysite nanotubes-decorated polyethersulfone ultrafiltration membrane modified with chitosan-silver nanoparticles, *Chem. Eng. J.*, 228 (2013) 12–20;
- (c) M. K. Sinha, M. K. Purkait, Use of CS–PAA nanoparticles as an alternative to metal oxide nanoparticles and their effect on fouling mitigation of a PSF ultrafiltration membrane, *RSC Adv.*, 5 (2015) 66109-66121.
- [20] B. Yu, F. Zhou, H. Y Hu, C. W. Wang, W. M. Liu, Synthesis and properties of polymer brushes bearing ionic liquid moieties, *Electrochim Acta.*, 53 (2007) 487-494.
- [21] Y. Ye, S. Sharick, Y. A. Elabd, Anion exchanged polymerized ionic liquids: high free volume single ion conductors, *Polymer*, 52 (2011) 1309-1317.
- [22] W. Qian, J. Texter, F. Yan, *Chem. Soc. Rev.*, 46 (2017) 1124-1159.
- [23] B. S. Lee, Y. S. Chi, J. K. Lee, Imidazolium ion terminated self-assembled monolayers on Au: effects of counter anions on surface wettability, *J Am Chem Soc.*, 126 (2004) 480-481.
- [24] Q. Ye, T. Gao, F. Wan, Grafting poly(ionic liquid) brushes for antibacterial and anti-biofouling applications, *J Mater Chem.*, 22 (2012) 13123-13131.
- [25] C. Du, X. Ma, C. Wu, Polymerizable ionic liquid copolymer P(MMA@co@BVIm@Br) and its effect on the surface wettability of PVDF blend membranes, *Chin J Polym Sci.*, 33 (2015) 857-868.
- [26] Y.-Y. Cheng, C.-H. Du, C.-J. Wu, K.-X. Sun, N.-P. Chi, Improving the hydrophilic and antifouling properties of poly(vinyl chloride) membranes by atom transfer radical polymerization grafting of poly(ionic liquid) brushes, *Polym Adv Technol.*, 29 (2018) 623–631
- [27] (a) A. Mollahosseini, A. Rahimpour, Interfacially polymerized thin film nanofiltration membranes on TiO<sub>2</sub> coated polysulfone substrate, *J. Ind. Eng. Chem.*, 20 (5) (2014) 1261-1268;
- (b) S. H. Kim, S.-Y. Kwak, B.-H. Sohn, T. H. Park, Design of TiO<sub>2</sub> nanoparticle self-assembled aromatic polyamide thin-film-composite (TFC) membrane as an approach to solve biofouling problem, *J. Membr. Sci.*, 211 (1) (2003) 157-165.
- [28] S. Pourjafar, A. Rahimpour, M. Jahanshahi, Synthesis and characterization of PVA/PES thin film composite nanofiltration membrane modified with TiO<sub>2</sub> nanoparticles for better performance and surface properties, *J. Ind. Eng. Chem.*, 18(4) (2012) 1398-1405.
- 29 a) R. F. M. Elshaarawy, T. B. Mostafa, A. A. Refaee, E. A. El-Sawi, Ionic Sal-SG Schiff bases as new synergetic chemotherapeutic candidates: synthesis, metalation with Pd(II) and in vitro pharmacological evaluation, *RSC Adv.*, 5 (2015) 68260-68269;
- (b) R. F. M. Elshaarawy, H. R. Z. Tadros, R. M. Abd El-Aal, F. H. A. Mustafa, Y. A. Soliman, M.A. Hamed, *J. Environ. Chem. Eng.*, 4 (2016) 2754-2764;
- (c) L. Carson, P. K. W. Chau, M. J. Earle, M. A. Gilea, B. F. Gilmore, S. P. Gorman, M. T. McCann, K. R. Seddon, *Green Chem.*, 11 (2009) 492-497.

- (d) R. F. M. Elshaarawy, I. M. Eldeen, E. M. Hassan, Efficient synthesis and evaluation of bis-pyridinium/bis-quinolinium metallosalophens as antibiotic and antitumor candidates, *J. Mol. Struct.*, 1128 (2016) 162-173
- [30] M. Padaki, A. M. Isloor, J. Fernandes, K. N. Prabhu, New polypropylene supported chitosan NF-membrane for desalination application, *Desalination*, 280 (2011) 419-423.
- [31] O. Iguerb, C. Poleunis, F. Mazéas, C. Compère, P. Bertrand, Antifouling Properties of Poly(methyl methacrylate) Films Grafted with Poly(ethylene glycol) Monoacrylate Immersed in Seawater, *Langmuir*, 24 (21) (2008) 12272-12281.
- [32] L. Liu, D. Y. W. Di, H. Park, M. Son, H.-G. Hur, H. Choi, Improved antifouling performance of polyethersulfone (PES) membrane via surface modification by CNTs bound polyelectrolyte multilayers, *RSC Adv.*, 5 (2015) 7340-7348.
- [31] Y. S. Zhou, L. J. Zhang, X. R. Zeng, J. J. Vital, X. Z. You, A new structurally characterized organotin/Schiff-base complex with approximately rectangular molecular boxes formed through hydrogen bonds, *J. Mol. Struct.*, 553 (2000) 25-30.
- [34] J. G. Yu, J. J. Fan, K. L. Lv, Anatase TiO<sub>2</sub> nanosheets with exposed (001) facets: improved photoelectric conversion efficiency in dye-sensitized solar cells, *Nanoscale*, 2 (2010) 2144-2149.
- [35] I.M. Wienk, R. M. Boom, M. A. M. Beerlage, Recent advances in the formation of phase inversion membranes made from amorphous or semicrystalline polymers, *J. Membr. Sci.*, 113 (1996) 361.
- [36] (a) R. Taylor, R. Krishna, *Multicomponent Mass Transfer* Vol. 597, Wiley New York (1993);  
(b) F. Zhang, W. Zhang, Y. Yu, B. Deng, J. Li, J. Jin, Sol-gel preparation of PAA-g-PVDF/TiO<sub>2</sub> nanocomposite hollow fiber membranes with extremely high water flux and improved antifouling property, *J. Membr. Sci.*, 432 (2013) 25-32.
- [37] T. Wang, Y. Wang, Y. Su, Z. Jiang, Antifouling ultrafiltration membrane composed of polyethersulfone and sulfobetaine copolymer, *J. Membr. Sci.*, 280 (2006) 343-350.
- [38] H. Yu, Y. Cao, G. Kang, J. Liu, M. Li, Tethering methoxy polyethylene glycols to improve the antifouling property of PSF/PAA-blended membranes, *J. Appl. Polym. Sci.*, 124 (2012) E123–E133.

## Graphical abstract



ACCEPTED MANUSCRIPT

---

### Highlights

- ✓ A practical synthetic route of poly ionic liquid-chitosan Schiff bases (PILCSB) is reported.
- ✓ PILCSB was employed for surface modification of polysulfone to give mixed matrix membranes (MMMs).
- ✓ Surface hydrophilicity of the MMMs was remarkably enhanced compared to the neat PSU membrane.
- ✓ Pure water flux recovery ratio (FRR) experiment showed higher water permeability for MMMs.
- ✓ BSA filtration experiment demonstrates promoted and promising antifouling performance for MMMs.